TopoBeam

Yuxin Lin*
University of Michigan

Mania Aghaei Meibodi*
University of Michigan

Kira Barton
University of Michigan

*All authors contributed equally to this research

Data-Informed Feedforward Control for Robotic 3D Concrete Printing of Topology Optimized Building Elements

1

1 Full-scale 1.2 m topology-optimized beam segment produced by robotic 3D concrete printing.

ABSTRACT

Reinforced concrete remains central to sustainable urban development, yet conventional casting is labor- and material-intensive due to formwork. Combining 3D Concrete Printing (3DCP) with topology optimization enables complex, efficient elements without formwork by depositing material only where structurally required. However, 3DCP of topology-optimized building elements (TOBEs)—often with multi-branch geometries—remains constrained by the inability to reliably start–stop extrusion during robotic traversal between discontinuous regions. Frequent start–stop events further risk hose clogging and pump build-up, particularly with fast-setting mixes. This research addresses these challenges through system upgrades and a feedforward input shaping strategy for automated start–stop 3DCP using a 1K system with a fast-setting mix. A pneumatic pinch valve was integrated into the printhead, with in-line sensors logging hose pressure, pumping power, and pump/valve states. Combined with geometric measurements, this data informed a model guiding printpath design while modulating pump rate and robot velocity, with thresholding applied to prevent clogging. The method was validated through benchmarking tests and full-scale robotic 3D concrete printing of a 1.2 m topology-optimized beam in Figure 1. Results showed uninterrupted printing without manual tuning, completing the segment in 45 minutes and saving 65% of material compared to a conventional beam. By compensating for pressure-related start–stop defects, the control method ensured consistent layer width with deviation less than 5 mm. This work establishes a foundation for adaptive control in robotic 3DCP, advancing scalability and repeatability for optimized components.

INTRODUCTION

Reinforced concrete (RC) (Aghaei Meibodi et al. 2018; Anton et al. 2021) will be pivotal in meeting the demands of sustainable urbanization, as it facilitates the construction of long-span, large-scale infrastructure and multi-story buildings. However, conventional concrete construction methods remain heavily dependent on formwork, making them inefficient in terms of material use, manufacturing time, labor, and overall cost. By integrating 3D Concrete Printing (3DCP) with computational material optimization methods (Sigmund 2000, Bi et al. 2022), it becomes possible to fabricate materially efficient and lightweight building elements without formwork, thereby minimizing concrete and reinforcement usage by placing them only where structurally required. Topology optimization (TO), a key computational method for material optimization (Bi et al. 2022), determines the most efficient material distribution based on performance criteria such as strength or weight, given specific loading and support conditions. By aligning material placement with force paths, TO enables structurally efficient, performance-driven design. While TO are widely utilized in fields such as aerospace and mechanical design applications to manufacture ultra-lightweight components that maximize structural performance, their full potential remains untapped in the realm of concrete construction applications.

Although 3DCP shows significant promise for the fabrication of topology-optimized building elements (TOBEs), its widespread adoption remains limited. TOBEs often feature complex geometries—such as overhangs and branching elements—that are challenging to 3D print in concrete (Aghaei Meibodi, Lin, and Chen 2024; Kamhawi and Aghaei Meibodi 2024). Achieving high geometric fidelity and dimensional accuracy in 3DCP of TOBEs requires both the capability to start-stop material extrusion during traverses between branches and the precise coordination of tool center point (TCP) velocity, extrusion rate, and toolpath design to avoid under- or over-extrusion at these moments. Furthermore, an effective approach to prevent clogging is essential, as flow interruptions trigger thixotropic structural build-up inside the hose. In the absence of shear, interparticle bonds reform, increasing yield stress and causing the material to stiffen more rapidly, while repeated interruptions increase residence time in the delivery system, further increasing the risk of blockage.

Meeting these fabrication conditions requires advanced sensing hardware and control capabilities over multiple subsystems, including the concrete pump, pinch valve, and robotic arm. Most current 3DCP systems lack integrated control for fabrication parameters, relying instead on operators to fine-tune the fabrication settings through manual, trial-and-error approach. This limits the repeatability and scalability of 3DCP. This paper contributes to addressing this gap by presenting: (a) physical system upgrades and (b) laying the foundation for the development of data-informed feedforward strategies, specifically input shaping approaches, that enable precise material deposition; thereby acting as a catalyst for the realization of the full potential of 3DCP for materially optimized elements, in particular TOBEs.

ROBOTIC 3DCP OF MATERIALLY OPTIMIZED BUILDING ELEMENTS

Approaches in Robotic 3DCP to Mitigate Fabrication Complexity in Multi-Branch Structures

The branching geometry of TOBEs creates discontinuous regions, or “islands,” that are difficult to fabricate with most current 3DCP systems—many of which lack frequent start-stop extrusion control. To address this limitation:

- TOBEs are frequently segmented into simpler, continuous parts without islands, which facilitates continuous material deposition. The segmented parts are manually assembled post-printing to form the complete building element (Vantyghem et al. 2020; Ooms et al. 2022; Gaudillière-Jami et al. 2019; Li et al. 2024; Akbarzadeh et al. 2024).
- Alternatively, traverse paths between the branches are considered part of the structure during 3DCP to eliminate the need to start-stop material extrusion. Here, intermediate connecting surfaces are introduced between branches to maintain printpath continuity during printing, which are subsequently removed (Ooms et al. 2022; Gaudillière-Jami et al. 2019).

Examples of existing approaches include the topology-optimized post-tensioned girder shown in Figure 2a, which was divided into nine island-free segments for individual printing and later post-tensioned assembly (Vantyghem et al., 2020), and the FloatArch project shown in Figure 2b, which had segmentation at branching regions with non-planar, stress-aligned interfaces (Li et al., 2024). Both projects reduce island printing but require precise post-assembly. The OptiBridge project in Figure 2c (Ooms et al. 2022) and XtreeE’s Krypton column in Figure 2d (Gaudillière-Jami et al. 2019) avoided start-stop events by printing stay-in-place or removable connecting surfaces between branches at the cost of extra material waste. The Diamanti Bridge project in Figure 2e (Akbarzadeh et al. 2024) minimized start-stop events through graph-based

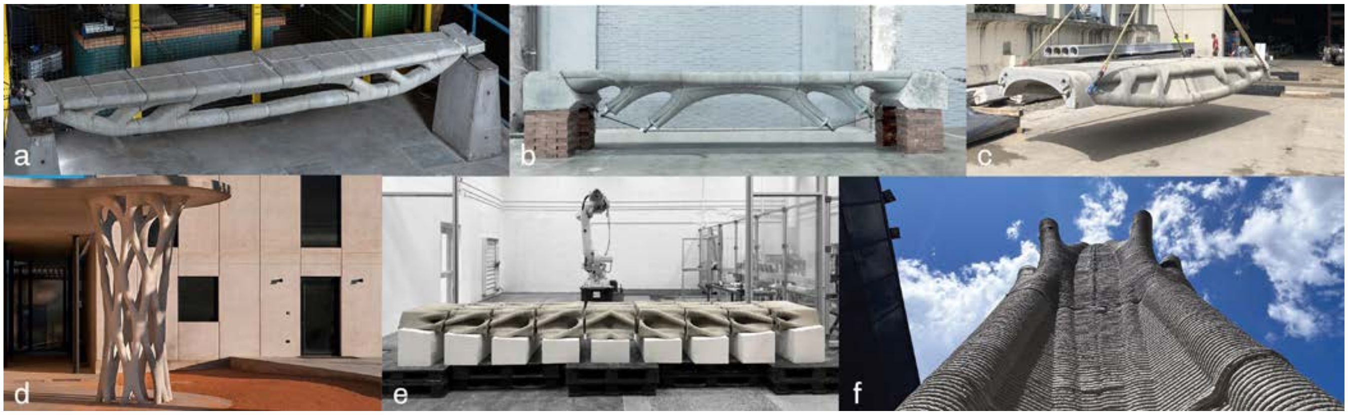

2 a: Topology optimized post-tensioned concrete girder (Vantyghem et al. 2020); b: A cable-supported, unreinforced, and re-assemblable 3D printed concrete structure (Li et al. 2024); c: Topology optimized concrete footbridge (Ooms et al. 2022); d: Krypton, a column in Aix-en-Provence (Gaudillière-Jami et al. 2019); e: 3D printed, post-tensioned concrete canopy (Akbarzadeh et al. 2024); f: Topology optimized BranchWall. (Lin, Bayramvand, and Aghaei Meibodi 2025) 2

path planning to merge islands where possible, and layer-stacking multiple layers of one branch before switching.

In the authors' Branch Wall project in Figure 2f (Lin, Bayramvand, and Aghaei Meibodi 2025), multi-island printing was achieved without segmentation by integrating a pinch valve and synchronizing pumping actuation with robotic motion. However, process parameters were manually tuned to prevent extrusion defects after traverses during the 3DCP process.

These studies have successfully expanded 3DCP research in the context of branching structures within TOBEs by exploring novel approaches to part segmentation, surface intervention, print-path planning, and manual tuning of process parameters to mitigate the challenges of printing branching features in complex geometries. The presented paper contributes to the field by introducing a data-informed feed forward control strategy to achieve automated robotic 3DCP of TOBEs, enabling the necessary stop and start of the printing process to fabricate islands.

3D Concrete Printing Systems

Successful 3DCP of TOBEs depends on controlling both open time—the workable period for pumping—and setting time—the period until the material transitions from plastic to rigid with sufficient yield strength to support subsequent layers. Setting time governs buildability, the ability of a freshly deposited layer to retain shape under its own weight and subsequent loads without collapse or deformation. Two primary strategies exist to ensure buildability behavior: (a) accelerating the setting time of the concrete used for 3D printing (Anton et al. 2021), or (b) employing a non-accelerated material for 3D printing while simultaneously and sequentially casting set-on-demand concrete to scaffold the 3D printed material (Aghaei Meibodi, Lin, and Chen 2024).

Existing 3DCP technologies primarily fall into two categories: one component (1K) and two component (2K) systems. They both can be employed for the manufacturing of TOBEs, but they have different capabilities. In both systems, a concrete slurry is pumped to the printhead for layer-by-layer deposition. The critical distinction lies in how each system controls the material's setting behavior. The 2K system entails an inline mixing capability in the printhead, enabling the introduction of a setting accelerator in the printhead that facilitates the rapid setting of concrete during extrusions (Wangler et al. 2024, Tao et al. 2024). In the 1K system, the printhead does not have mixing capabilities; if there is a desire to have control over setting time, an accelerator is added to the concrete mix at the pumping stage and the material delivery time should account for the transportation from the pump to the printhead via a hose and eventually to the extrusion point.

Research Set-up and Challenges: One Component 3D Printing with Start-stop Mechanisms and Fast-Setting Material

This research employs the 1K 3DCP setup, paired with Sikacrete®-752, a pre-blended concrete dry mix containing a setting accelerator for rapid setting upon contact with water ("Sika" 2025). Start-stop control is enabled via a pneumatic pinch valve at the printhead, synchronized with pump rate adjustments. Extrusion is stopped by simultaneously closing the valve and setting the pump rotational frequency to 0 Hz. To resume extrusion, the valve is opened while restoring the pump frequency to its pre-stop value.

The combination of start–stop operation and the

3 Image of a 4.5 m topology-optimized beam with load-bearing support at both ends, highlighting the 3D-printed segment (in blue) with complex geometries. 3

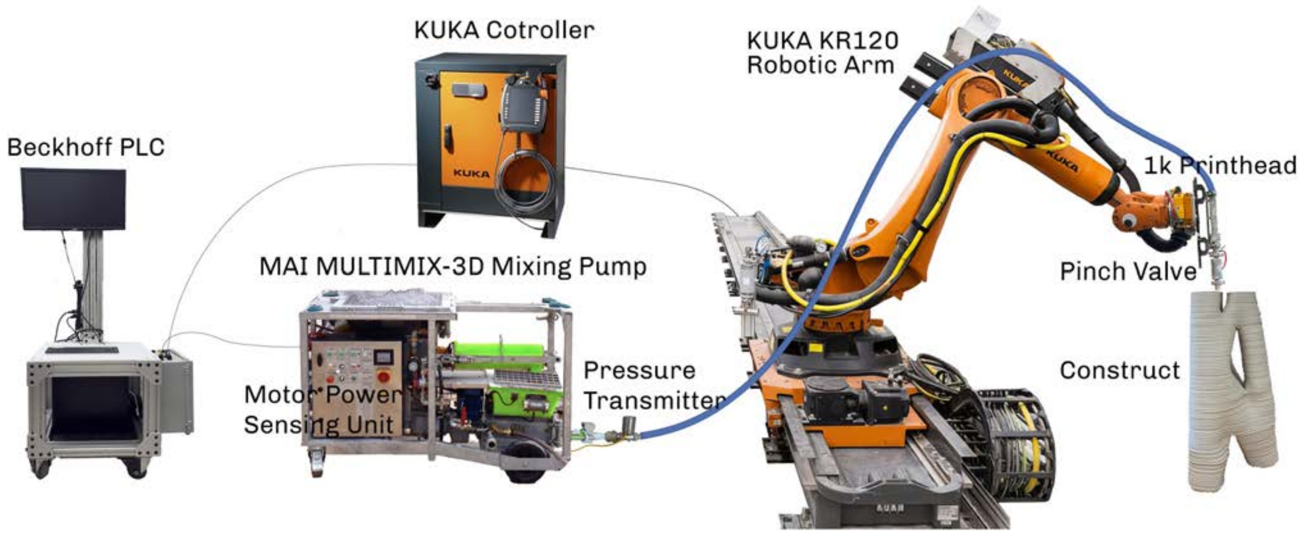

4 The 3D concrete printing fabrication system setup presented in this research consists of: the MAI MULTIMIX-3D Mixing Pump (MAI pump), functioning as the primary slurry mixer and delivery unit; a pinch valve integrated into the printhead to rapidly halt material flow; and a KUKA KR120 robotic arm, providing six degrees of freedom for spatial positioning. The sensors integrated in the system include: a pressure transmitter (0–40 bar) and internal motor power sensing unit. 4

fast-setting nature of the accelerated mix demands precise coordination between robot TCP speed, pumping flow rate, valve actuation, and printpath design. This entails.

- Managing extrusion post-closure residual slug when the pinch valve closes, as a slug of mortar inside the pinch valve is pushed out immediately when the pinch valve closes.
- Compensating for material under-extrusion when the pinch valve reopens and the pump must re-pressurize the delivery hose to stabilize the material flow.
- Maintaining a pumping rate above the clogging threshold and monitoring the clogging anomaly during the process, while fine-tuning TCP speed to achieve the required layer width and ensure sufficient layer time for structural build-up.

METHODS

This methods section presents an integrated start–stop control strategy for 1K robotic 3DCP that preserves geometric fidelity and prevents clogging. The strategy applies a data-informed feedforward input shaping, using static parameter mappings based on measured extrusion defects (over/under-extrusion) to pre-shape input parameters informed by in-line data collection. This includes:

- Integrating sensors into the robotic 3DCP system and defining key data-collection points.
- Implementing input shaping to inform printpath design and coordinate the robot TCP velocity, the pump rotational frequency (which sets the pumping flow rate), and the pinch valve on/off actuation.
- Establishing flow rate thresholds and continuously monitoring for clogging risk throughout the 3D printing process.

The method is developed through test printing to determine suitable parameters, followed by validation through the final 1:1 scale manufacturing of a topology optimized beam segment, as shown in Figure 3.

Integrated Sensing and Control Framework for 1K 3DCP

Sensor selection and placement: The monitoring framework focuses on variables that directly characterize material flow within the delivery hose, including hose inlet pressure and pumping power, as shown in Figure 4. Hose pressure is considered the primary indicator of pumping conditions, as it must exceed the material's yield threshold before steady-state flow is established (Roussel, Lanos, and Toutou, 2006). A pressure transducer is installed at the pump outlet to capture head losses representative of the entire delivery line. Pumping power is obtained from the MAI MultiMix-3D mixing pump's (MAI pump) integrated controller, providing a complementary measure of mechanical energy input to the extrusion process.

Communication architecture and centralized control: The centralized coordination of the 3DCP system is implemented on a Beckhoff programmable logic controller (PLC) running TwinCAT automation software. Figure 4 shows this platform coordinates three primary subsystems: (a) a KUKA KR120 industrial robot, (b) MAI pump, and (c) a pneumatically actuated pinch valve. The robot streams pre-programmed TCP velocity profiles and pump/valve command signals to the PLC over industrial Ethernet. Bidirectional communication between the MAI pump and TwinCAT is achieved via OPC-UA, enabling the transmission of pressure and pumping power signals from the MAI pump's controller to TwinCAT, and the dispatch of pump rotational frequency and on/off commands from TwinCAT to the pump. The pinch valve is actuated through the PLC's digital I/O channels to ensure real-time responsiveness. This integrated architecture ensures that TCP motion, pump operation, and valve actuation are synchronized within a unified control timeline.

Data acquisition and storage: All process variables—including hose pressure, pumping power, robot TCP velocity, pump rotational frequency, and valve state—are logged within a unified temporal framework in TwinCAT. Each signal is resampled to a fixed 50 Hz rate and time-stamped using the PLC's internal clock, ensuring precise alignment across data streams. The synchronized dataset is recorded in CSV format to support offline analysis. This structured logging methodology ensures reproducible temporal correlation between process events and observed printing outcomes, facilitating detailed post-process evaluation of system performance.

Data-Informed Compensation of Valve-Induced Over-Extrusion and Pressure-Triggered Extrusion Restarts

Start–stop cycles in 3DCP introduce two systematic defects related to the over-extrusion and under-extrusion during cycling, which will significantly affect the geometrical accuracy and buildability of the parts during the 3DCP process.

Control strategy for extrusion sequences. During extrusion stop sequences, a valve post-closure residual slug is released immediately after the pump-off and valve-close command, shown in Figure 5. As a result, the extruded filament exhibits a transient width spike. To mitigate this effect, a lead-out segment is appended to the print path after the valve-close command. The robot accelerates to a predetermined speed over this segment to stretch the residual slug over a short distance. The lead-out distance, $L_{\text{lead-out}}$, is calculated as Equation 1:

$$L_{\text{lead-out}} = V_{\text{lead-out}} \times T_{\text{value}} \tag{1}$$

where $V_{\text{lead-out}}$ is the robot travel speed during the lead-out printpath and T_{valve} is the measured valve response time. If the control volume of the valve is N, approximately N/3 material volume is discharged during T_{valve}. The required lead-out speed to maintain the target cross-sectional area A_{target}, can then be calculated as Equation 2:

$$V_{\text{lead-out}} = \frac{N/3}{A_{\text{target}} \times T_{\text{valve}}}, \quad \text{as} \quad A_{\text{target}} = C \times H \times W_{\text{target}} \tag{2}$$

where C is a shape factor accounting for the non-rectangular filament cross-section, H is the layer height which is constrained by the nozzle height (10 mm), W_{target} is the target filament width. This equation ensures that the deposition accounts for the release of the residual slug, minimizing its visual and structural impact on the printed filament.

Control strategy for extrusion restart sequences: During extrusion restart sequences, the pumping stops while the pressure of the hose starts to drop from its original value; thus requiring the pinch valve closure to maintain the pressure at a lower equilibrium level. When pumping resumes and the valve reopens, the pressure begins to rise back toward its peak while the material flow recovers to the target filament dimension. We characterize the restart phase by measuring three variables for each start–stop cycle: the peak pressure P_{peak} to initiate stable material flow, the reduced equilibrium pressure during valve closure P_{low}, and the pressure recovery time T_{recovery}. T_{recovery} is defined as the duration required for the pressure to increase from P_{low} to P_{peak}. The observed recovery behavior follows a first-order profile given in Equation 3:

$$P(t) = P_{\text{peak}} - (P_{\text{peak}} - P_{\text{low}}) \times e^{-t/\lambda} \tag{3}$$

where λ is a time constant that depends on system

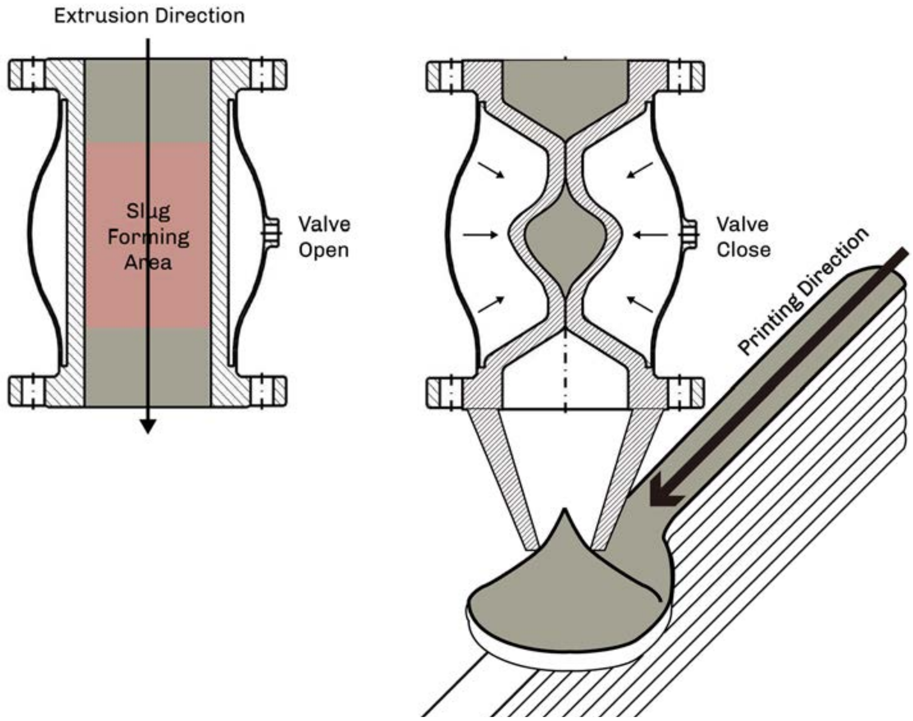

5

5 Schematic illustration of slug formation in a pneumatic pinch valve during the process: Upon valve closure, the residual material inside the pinch valve is expelled as a pressurized slug, resulting in a localized over-deposition at the start of the next print segment if not compensated.

characteristics. This expression is included to describe the recovery dynamics; however, we directly use the measured recovery time $T_{recovery}$ for the subsequent calculation of the lead-in distance.

To evaluate the effect of the recovery on printed geometry, we measured the minimum filament width $W_{minimum}$ over the recovery period from printed filaments. The deviation of $W_{minimum}$ from the target width W_{target} indicates whether the printing speed should be increased or decreased. The adjusted speed $V_{lead\text{-}in}$ is then calculated using Equation 4:

$$V_{\text{lead-in}} = V_{\text{printing}} \times \frac{W_{\text{target}}}{W_{\text{minimum}}} \tag{4}$$

where $V_{printing}$ is the nominal printing speed used during steady-state extrusion. The corresponding lead-in print-path length $L_{lead\text{-}in}$ is then computed using Equation 5:

$$L_{\text{lead-in}} \propto (T_{\text{recovery}} \times V_{\text{lead-in}}) \tag{5}$$

This approach provides a direct, geometry-based correction to the lead-in robot TCP speed, ensuring that the filament width during pressure recovery matches the target width and preserves geometric accuracy in the printed filament.

Balancing Pumping Stability and Structural Build-Up

This section describes the strategy used to prevent clogging while ensuring necessary structural build-up in 1K 3DCP through in-line data collection of hose-inlet pressure and pump power. A pressure ceiling (26-30 Bar based on the pump use guidelines) is applied as an indicator that the material's yield stress has risen to a point where pumping becomes difficult and hardened material may begin to accumulate on the walls of the hopper. Sudden spikes in pump power are treated as an early warning of material hardening that can gradually lead to clogging. Both anomaly detection approaches have been demonstrated in prior work (Lin and Aghaei Meibodi 2025).

Through extrusion testing, collected pressure and pump power data are used to determine a minimum safe pumping flow rate that ensures the material clears the hose and nozzle before a blockage can form. Moreover, the yield stress τ_y can be estimated from the measured maximum pressure required to initiate material flow using a simplified form of the Buckingham–Reiner equation (Chen et al. 2022, Polychronopoulos et al. 2023), which is valid for high yield stress materials where viscous losses are small. For a cylindrical hose, the relationship is defined in Equation 6:

$$\tau(y) \approx \frac{R}{2L}\Delta P \tag{6}$$

where R is the hose inner radius (m), L is the hose length (m), and ΔP is the measured pressure drop along the hose (the pressure at the outlet of the hose can be considered

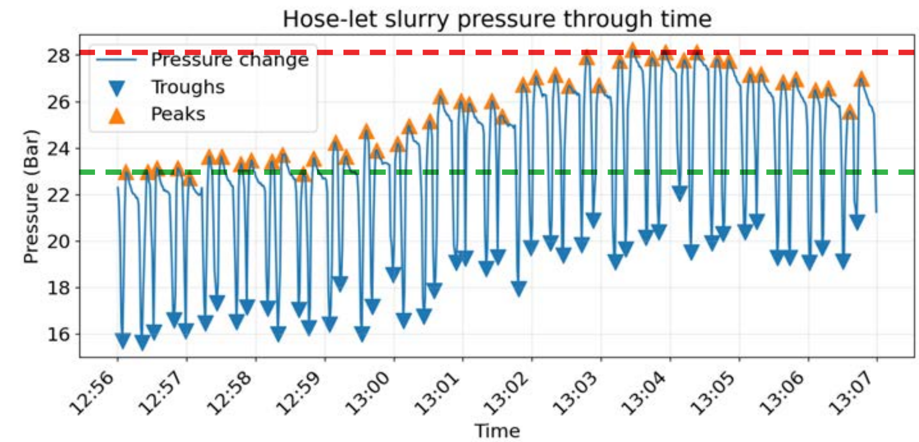

6

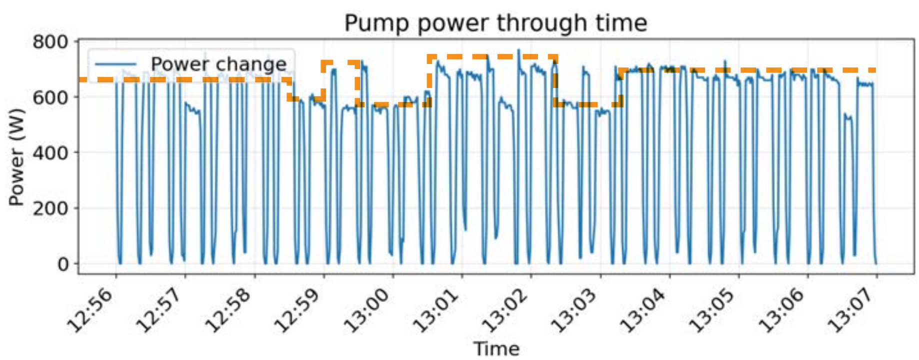

7

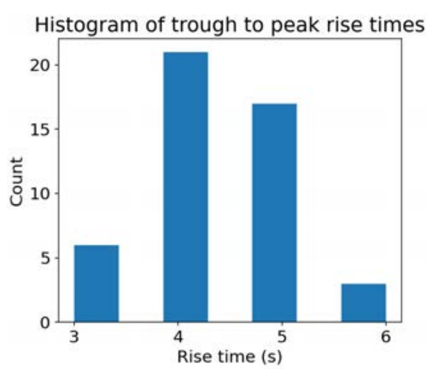

8

6 Hose-inlet slurry pressure during a 10-minute benchmark trial with 50 start–stop cycles at 25 Hz pump speed (2.2 L/min), showing peaks during deposition and troughs during traverses. The green line indicates a health pressure below 26 bar initially, whereas the later rise to 28 bar, shown in red, signals an increased risk of clogging..

7 Pump power data during the initial benchmark printing test at 22 Hz pump speed (2.2 L/min). Intermittent power spikes, as highlighted by the orange line, indicate increased effort by the pump.

8 Histogram of pressure recovery times (trough-to-peak) indicates a minimum of 3 s, a maximum of 6 s, and an average of 4.36 s.

as none). This estimated yield stress is used to determine the minimum layer time for buildability by ensuring that the material strength gained after deposition is sufficient to support subsequent layers without collapse or excessive deformation. The robot TCP velocity is then calculated to balance both the geometric requirement for the target layer width and the build-up constraint.

RESULTS AND DISCUSSION

We validated the start–stop control strategy for 1K robotic 3DCP by (a) characterizing pressure dynamics for valve-induced extrusion, (b) monitoring pressure and pump power to balance pumpability with structural build-up, and (c) applying a geometry-informed feedforward input shaping to adjust the length and TCP velocity during lead-in and lead-out.

Pressure Dynamics During Start-stop Moments

The first set of tests involved printing the bottom portion of the beam as a benchmark trial. This test included repeated start–stop cycles over a 10-minute period, with approximately 50 cycles in total. The pump rotational frequency was set to 25 Hz, corresponding to a pumping flow rate of 2.2 L/min.

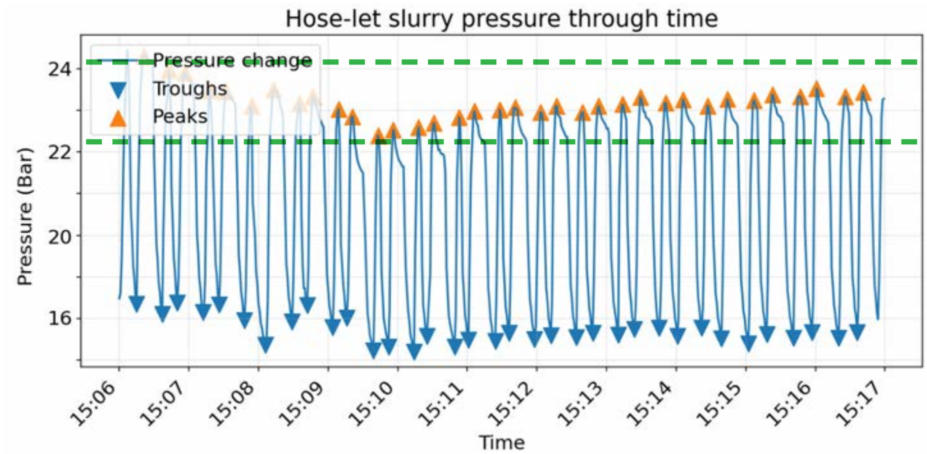

(a)

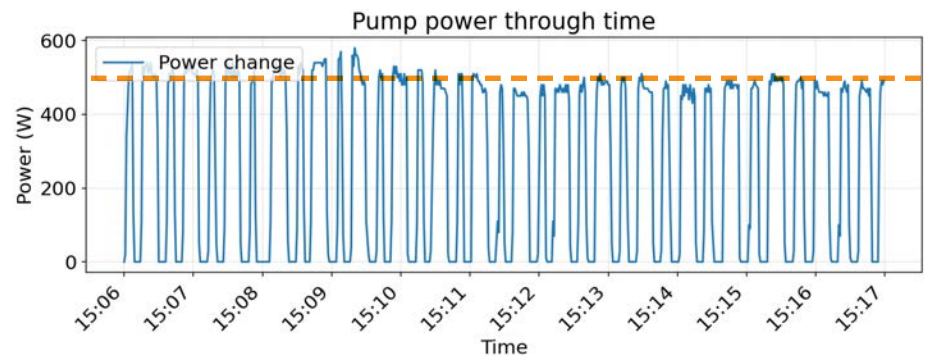

(b)

9

9 Pump pressure (a) and power data (b) during the adjusted printing trial at 29 Hz pump speed (2.5 L/min). Green lines indicate that pressure is always under 24 bar, which is healthy. And power output remained stable as indicated by the orange lines, confirming that the increased pumping rate reduced clogging risk while maintaining consistent material delivery.

Pressure data was collected continuously at 50 Hz. The data showed cyclic peaks during active deposition and troughs during traversal moves in Figure 6. When the pump was turned off and the valve closed, the pressure rapidly dropped by 8–10 bar. Upon restarting, the pressure increased back to the operating level. The histogram of recovery times in Figure 8 indicated a minimum of 3 s, a maximum of 6 s, and an average of 4.36 s. This average recovery time, $T_{recovery}$, was later used in Equation 5 to define the required lead-in distance for consistent deposition.

Balancing Pumpability and Structural Build-Up with Pressure/Power Monitoring

To prevent clogging while maintaining structural build-up, we monitored both hose pressure and pump power as early-warning indicators. Benchmark tests established the minimum safe pumping flow rate needed to clear the line before clogging.

During the first test, the maximum hose-inlet pressure rose from an initial 23 bar to 28 bar in Figure 6. This increase suggested that material was not being expelled quickly enough, allowing yield stress to increase to a level that risked blockage. Pump power data in Figure 7 also showed intermittent spikes, indicating additional effort by the pump. In response, the pump speed was increased from 22 Hz to 29 Hz, which raised the flow rate from 2.2 L/min to 2.5 L/min. At this rate, inlet pressure in Figure 9a remained below 24 bar and pump power stayed stable in Figure 9b during a subsequent 10 minute test, confirming that the adjusted flow rate reduced clogging risk.

Using Equation 6, we conservatively estimated the material yield stress from the measured pressure. For a hose length of 10 m and inner diameter of 25.4 mm, the lowest recorded peak pressure of 23 bar gave an estimated yield stress of 2.86 kPa. This value was sufficient to support several partially overlapping overhanging layers immediately after deposition. Given the material's fast-setting properties, buildability was considered suitable for the printing scenario.

Feedforward Compensation for Start–Stop Control

Lead-out printpath design (residual slug control): With a pumping rate of 2.5 L/min and a TCP velocity of 150 mm/s, the target cross-sectional area A(target) was 278 mm². The pinch valve (AKO VMC DN 25) has a control volume N = 90 ml and closure time T_{valve} = 200 ms. Using Equation 2, the required lead-out speed $V_{lead\text{-}out}$ was calculated as 540 mm/s to spread the residual slug without exceeding A_{target}. Equation 1 then gave a lead-out distance $L_{lead\text{-}out}$ of 108 mm. However, the jump from 150 mm/s to 540 mm/s induces

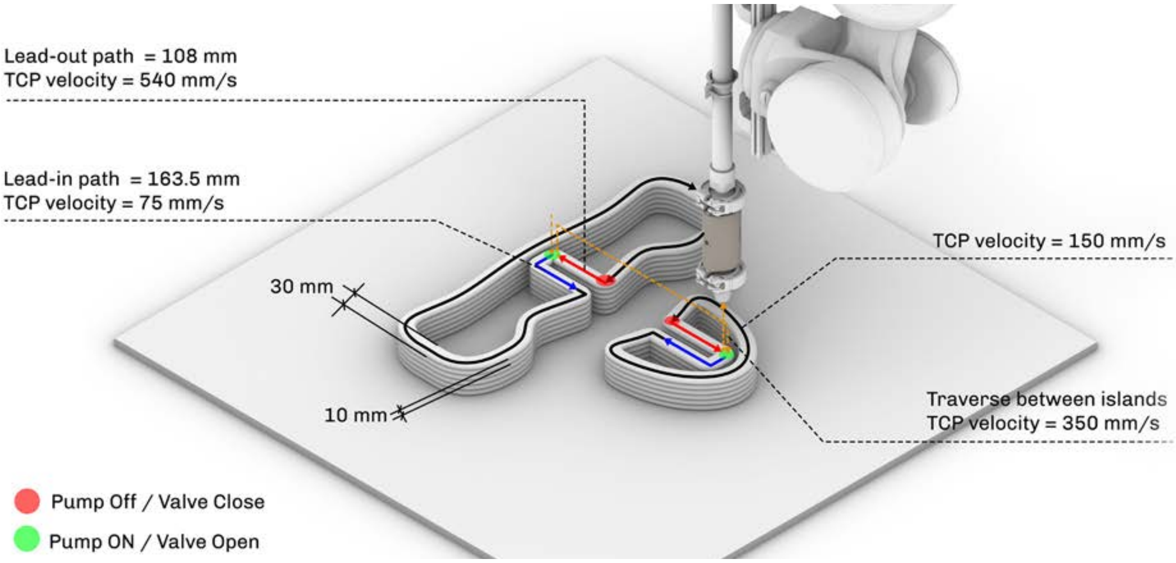

10

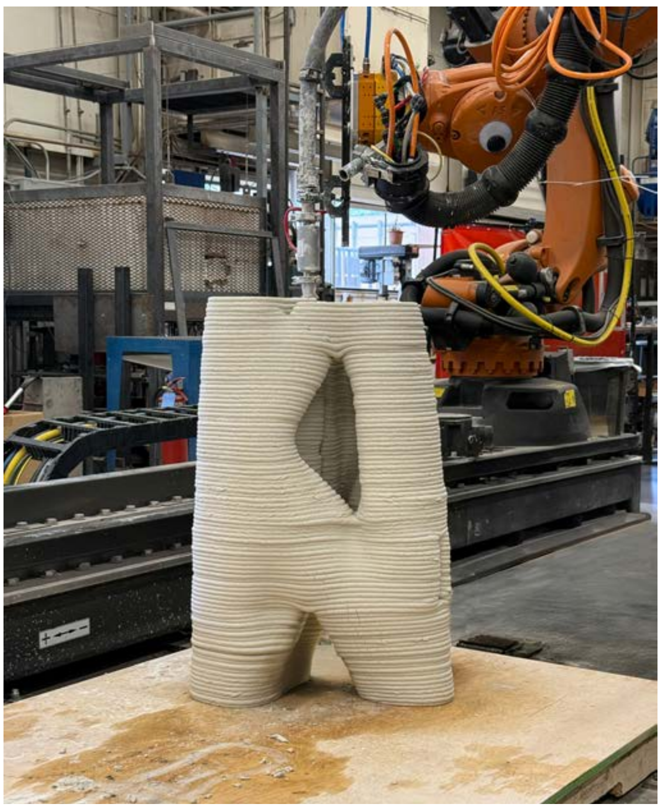

11

12

high acceleration and deceleration of the robotic arm, which can cause vibrations affecting deposition stability. While not critical in our tests, future work could incorporate feedforward or input-shaping strategies to smooth these transitions and reduce dynamic disturbances.

Lead-in printpath design (pressure recovery): When restarting, the pump and valve were actuated simultaneously. Empirical observations showed that, if the TCP velocity remained constant, the deposited filament width initially dropped to about half of the target value, and restoring the target width required approximately half of the recovery time $T_{recovery}$. Through the Equation 4, $V_{lead\text{-}in}$ was set to half of the normal TCP velocity. Equation 5 then gave a lead-in path length of 163.5 mm. These derived parameters were applied during the full-scale beam fabrication, as shown in Figure 10.

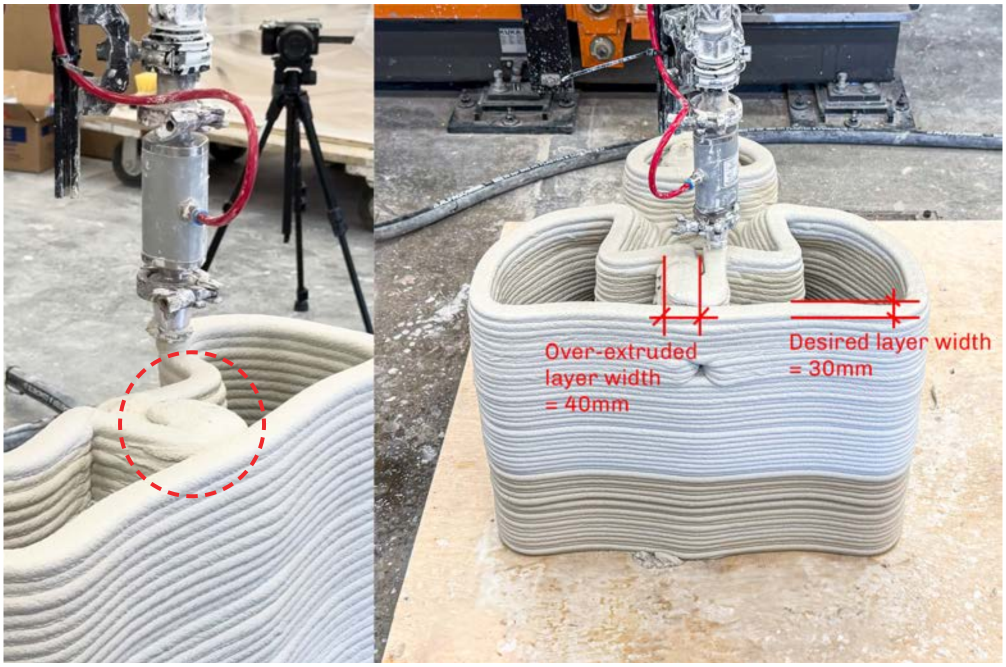

13

10 Illustration of TCP velocity modulation and start-stop control logic. Lead-in and lead-out segments have varied robot speed in relation to valve/pump timing to ensure consistent material deposition across islands.

11 Start–stop 3D printing of a full-scale 3D-printed topology-optimized beam segment using the proposed feedforward control strategy.

12 The final printed beam with complex branching zones. This image demonstrates consistent layer quality and high geometric precision at branching zones.

13 Close-up views of lead in and lead out zones during the 3D concrete printing of the topology optimized beam. Localized over-extrusion was still observed during some lead-in printpaths as indicated in the red circle. The layer width increased from the desired 30mm to 40mm.

Full-scale Validation on a Topology-Optimized Beam Segment

The developed control strategy enabled uninterrupted 3D printing of a 1.2 m beam segment using only 226 kg of material and 45 minutes of printing time, with no manual tuning of process parameters, as shown in Figure 11. The feedforward input shapping method determined suitable TCP velocity, and lead-in/lead-out timing and length, as well as precise signal synchronized for actuating the pinch valve and toggling the pump rotational frequency This coordination allowed for a fully automated printing process without the need for manual interruptions or manual parameter tuning during the 3DCP process, as well as robust start-stop cycles with consistent material flow for the overall geometry shown in Figure 12.

However, localized over-extrusion was still observed during some lead-in printpaths in Figure 13. Analysis of a 7-minute pressure segment corresponding to these defects in Figure 14 revealed that while P_{peak} varied only slightly (20–22 bar), the minimum P_{low} varied more significantly (around 7 bar) than the benchmark test. The histogram showed an average recovery time of 4.86 s, with a shortest time of 2.76 s and a longest of 6.35 s. Higher P_{low} resulted in shorter recovery times, causing material flow to resume faster than expected, leading to over-extrusion when the TCP velocity was not adjusted accordingly.

Although explanation of these variations requires further study, certain trends were identified in the data. However, these should not be interpreted as definitive relationships; rather, they represent our working hypotheses informed by the observed patterns:

- Traverse time: Shorter traverse lengths—defined as the distance between the lead-out point of one island and the lead-in point of the next—were observed to correlate with smaller pressure drops. This association suggests a potential reduction in the time required to re-establish required pressure levels before extrusion resumes.
- Time-dependent rheology: As the fresh concrete continued to set, increases in yield stress affected the observed pressure behavior. This evolution appeared to be associated with higher operating pressures during printing and more pressure losses during start–stop events, potentially extending the time needed to re-pressurize the delivery hose.

These hypotheses underscore the need for systematic investigation into the coupling between process-induced variations and the time-dependent rheological behavior of the material. They also highlight the need for a closed-loop feedback control strategy capable of adapting process parameters in real time based on in-line measurements.

CONCLUSION

This research advances robotic 3DCP of topology-optimized building elements by addressing the key challenge of reliable start–stop extrusion during discontinuous printpaths. For hardware, we introduced a system

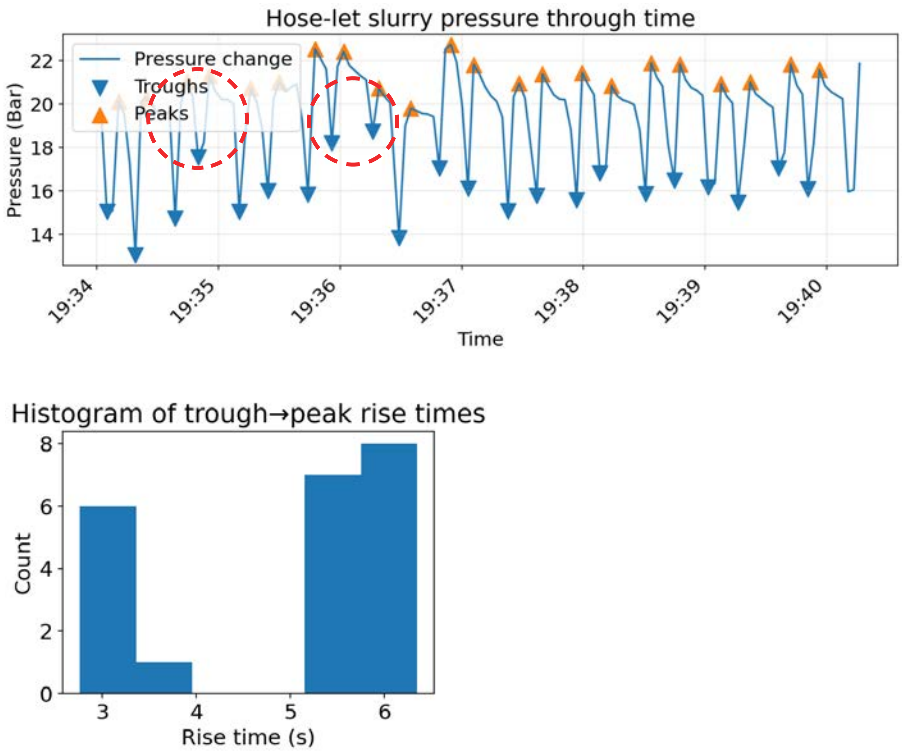

(a)

(b)

14 Pressure data (a) and histogram of recovery time distribution (b) within a 7-minute plot, corresponding to observed over-extrusion moments during the lead-in movements. As indicated in the red circles, P_{low} varied more significantly (13 bar to 19 bar), thus resulting in a shortest $T_{recovery}$ less than 3 s.

14

upgrade through the integration of a pneumatic pinch valve and synchronized communication framework across subsystems. Building on this foundation, we developed a feedforward input shaping strategy that uses static parameter mappings—derived from pump pressure, power, and measured extrusion defects—to pre-shape robot and pump inputs during lead-in and lead-out printpaths. This feedforward strategy mitigates transient over- and under-extrusion, enabling repeatable fabrication of complex branching geometries without manual tuning.

The successful full-scale fabrication of a topology-optimized beam segment with high fidelity and minimal intervention demonstrates a reproducible framework for automated 3DCP for material efficient structures in real-world applications. This work shows that predictive input shaping can effectively bridge the gap between complex geometric design and process execution. Future research will move beyond static input shaping toward the development of a control model that characterizes the dynamic relationships between process parameters and outcomes. Embedding such a model within a closed-loop controller will enable the system to identify optimal inputs in real time, advancing toward robust and intelligent automation in 3DCP.

ACKNOWLEDGEMENTS

The authors gratefully acknowledge Sika for sponsoring the material used in this research. Special thanks are extended to Yichuan Li for his assistance with the printpath generation and the initial printing process. We would also like to thank Jutang Gao, Christopher Watson, and Abdallah Kamhawi for their support in testing and in carrying out the final printing process.

REFERENCES

Aghaei Meibodi, Mania, Andrei Jipa, Rena Giesecke, Demetris Shammas, Mathias Bernhard, Matthias Leschok, Konrad Graser, and Benjamin Dillenburger. 2018. Smart Slab: Computational Design and Digital Fabrication of a Lightweight Concrete Slab. https://doi.org/10.52842/conf.acadia.2018.434.

Aghaei Meibodi, Mania, Yuxin Lin, and Hao Chen. 2024. "Hybrid Approaches Towards 3D Concrete Printing for Lightweight Reinforced Concrete Structures." Digital Concrete 2024 – Supplementary Proceedings. https://doi.org/10.24355/dbbs.084-202408140649-0.

Akbarzadeh, Masoud, Hua Chai, Yefan Zhi, Maximilian E. Ororbia, Teng Teng, Mathias Bernhard, Damon (Mohammad) Bolhassani, et al. 2024. "Diamanti: 3D-Printed, Post-Tensioned Concrete Canopy." In Fabricate 2024: Creating Resourceful Futures, 292–301. UCL Press. https://doi.org/10.2307/jj.11374766.40.

Anton, Ana, Lex Reiter, Timothy Wangler, Valens Frangez, Robert J. Flatt, and Benjamin Dillenburger. 2021. "A 3D Concrete Printing Prefabrication Platform for Bespoke Columns." Automation in Construction 122: 103467. https://doi.org/10.1016/j.

autcon.2020.103467.
Bi, Minghao, Phuong Tran, Lingwei Xia, Guowei Ma, and Yi Min Xie. 2022. “Topology Optimization for 3D Concrete Printing with Various Manufacturing Constraints.” Additive Manufacturing 57: 102982. https://doi.org/10.1016/j.addma.2022.102982.
Chen, Yu, Shan He, Yidong Gan, Oğuzhan Çopuroğlu, Fred Veer, and Erik Schlangen. 2022. “A Review of Printing Strategies, Sustainable Cementitious Materials and Characterization Methods in the Context of Extrusion-Based 3D Concrete Printing.” Journal of Building Engineering 45 (103599): 103599. https://doi.org/10.1016/j.jobe.2021.103599.
Gaudillière-Jami, Nadja, Romain Duballet, Charles Bouyssou, Alban Mallet, Philippe Roux, Mahriz Zakeri, and Justin Dirrenberger. 2019. “Large-Scale Additive Manufacturing of Ultra-High-Performance Concrete of Integrated Formwork for Truss-Shaped Pillars.” In Digital Concrete: Proceedings of the 1st RILEM International Conference on Concrete and Digital Fabrication, 459–472. Springer. https://doi.org/10.1007/978-3-319-92294-2_35.
Kamhawi, Abdallah, and Mania Aghaei Meibodi. 2024. “Techniques and Strategies in Extrusion-Based 3D Concrete Printing of Complex Components to Prevent Premature Failure.” Automation in Construction 168: 105768. https://doi.org/10.1016/j.autcon.2024.105768.
Li, Yu, Hao Wu, Xinjie Xie, Liming Zhang, Philip F. Yuan, and Yi Min Xie. 2024. “FloatArch: A Cable-Supported, Unreinforced, and Re-Assemblable 3D-Printed Concrete Structure Designed Using Multi-Material Topology Optimization.” Additive Manufacturing 81: 104012. https://doi.org/10.1016/j.addma.2024.104012.
Lin, Yuxin, Alireza Bayramvand, and Mania Aghaei Meibodi. 2025. “Towards Lightweight Structure: Coupling Topology Optimization with Non-Planar 3D Concrete Printing.” In, 3–12. https://doi.org/10.1007/978-981-96-3433-0_1.
Lin, Yuxin, and Mania Aghaei Meibodi. 2025. “Integrated Sensing Printhead: In-Line Data Collection for Non-Planar 3D Concrete Printing.” In ACADIA 2024: Designing Change, edited by Alicia Nahmad-Vazquez, Jason Johnson, Joshua Taron, Jinmo Rhee, Daniel Hapton, 355–64.
Ooms, Ticho, Gieljan Vantyghem, Yaxin Tao, Michiel Bekaert, Geert De Schutter, Kim Van Tittelboom, and Wouter De Corte. 2022. “The Production of a Topology-Optimized 3D-Printed Concrete Bridge.” In Digital Concrete 2022: Proceedings of the Third RILEM International Conference on Concrete and Digital Fabrication, 37–42. Springer. https://doi.org/10.1007/978-3-031-06116-5_6.
Polychronopoulos, Nickolas D., Ioannis E. Sarris, Lefteris Benos, and John Vlachopoulos. 2023. “Pressure Drop in Converging Flows in Three-Dimensional Printing of Concrete.” Physics of Fluids (Woodbury, N.Y.: 1994) 35 (9). https://doi.org/10.1063/5.0168928.
Roussel, Nicolas, Christophe Lanos, and Zahia Toutou. 2006. “Identification of Bingham Fluid Flow Parameters Using a Simple Squeeze Test.” Journal of Non-Newtonian Fluid Mechanics 135 (1): 1–7. https://doi.org/10.1016/j.jnnfm.2005.12.001.
Sigmund, Ole. 2000. “Topology Optimization: A Tool for the Tailoring of Structures and Materials.” Philosophical Transactions of the Royal Society A: Mathematical, Physical and Engineering Sciences 358 (1765): 211–227. https://doi.org/10.1098/rsta.2000.0528.
Sika. 2025. “3D Concrete Printing.” https://usa.sika.com/en/construction/concrete/3d-concrete-printing.html.
Tao, Yaxin, Kim Van Tittelboom, A. V. Rahul, Timothy Wangler, Ena Lloret-Fritschi, Robert J. Flatt, and Geert De Schutter. 2024. “Static Mixing for Set-on-Demand of Digital Concrete.” In RILEM Bookseries, 107–15. Cham: Springer Nature Switzerland. https://doi.org/10.1007/978-3-031-70031-6_13.
Vantyghem, Gieljan, Wouter De Corte, Emad Shakour, and Oded Amir. 2020. “3D Printing of a Post-Tensioned Concrete Girder Designed by Topology Optimization.” Automation in Construction 112: 103084. https://doi.org/10.1016/j.autcon.2020.103084.
Wangler, Timothy, Yaxin Tao, Arnesh Das, Matineh Mahmoudi, Seyma Gürel, and Robert J. Flatt. 2024. “Aluminate 2K Systems in Digital Concrete: Process, Design, Chemistry, and Outlook.” Cement and Concrete Research 185 (107644): 107644. https://doi.org/10.1016/j.cemconres.2024.107644.

IMAGE CREDITS

Figure 2: a © Vantyghem et al. 2020; b @ Li et al. 2024; c @ Ooms et al. 2022; d @Gaudillière-Jami et al. 2019; e @ Akbarzadeh et al. 2024.
All other drawings and images by the authors.

Yuxin Lin is a Ph.D. candidate at DART Lab within the Taubman College of Architecture and Urban Planning at the University of Michigan. His research focuses on advancing Robotic 3D Concrete Printing techniques alongside real-time control through the collection of live data. His work aims to facilitate the manufacturing of optimized and high-definition concrete components for use in the construction and building sectors.

Dr. Mania Aghaei Meibodi is Assistant Professor of Architecture at the University of Michigan's Taubman College of Architecture and Urban Planning. She leads the DART laboratory, where they innovate integrative computational design methods with robotic construction and 3D printing to tackle real-world construction challenges. Her interdisciplinary research focuses on computational design, robotic construction, large-scale 3D printing, and novel building materials.

Dr. Kira Barton is a professor of mechanical engineering, professor of robots, and Miller Faculty Scholar at the University of Michigan. Her primary research focus is on precision coordination and motion control for emerging applications, with a specialization in iterative learning control. Barton's work intersects controls and manufacturing and combines innovative manufacturing processes with enhanced engineering capabilities.